ELSEVIER

Materials Science and Engineering B 149 (2008) 41–46

MATERIALS SCIENCE & ENGINEERING B

www.elsevier.com/locate/mseb

# Synthesis, characterization, photoluminescence and ferroelectric properties of $PbTiO_3$ nanotube arrays

Lifeng Liu [a,b,*], Tingyin Ning [a,b], Yan Ren [a,b], Zhihui Sun [a,b], Feifei Wang [a,b], Weiya Zhou [a], Sishen Xie [a,**], Li Song [a,b], Shudong Luo [a,b], Dongfang Liu [a,b], Jun Shen [a,b], Wenjun Ma [a,b], Yueliang Zhou [a]

[a] *Beijing National Laboratory for Condensed Matter Physics & Institute of Physics, Chinese Academy of Sciences, Beijing 100080, People's Republic of China*

[b] *The Graduate School of Chinese Academy of Sciences, Beijing 100049, People's Republic of China*

Received 17 July 2007; received in revised form 21 November 2007; accepted 1 December 2007

**Abstract**

$PbTiO_3$ nanotube arrays have been synthesized via sol–gel template method, and their morphology and structures have been determined by scanning electron microscopy (SEM), X-ray diffraction (XRD) and transmission electron microscopy (TEM). The diameter and length of these nanotubes are about 300 nm and 50 μm, respectively, and their wall thickness is typically several tens of nanometers. XRD data shows that as-prepared PTO nanotubes possess perovskite structure, and electron diffraction demonstrates that they are polycrystalline. Photoluminescence spectrum of PTO nanotubes reveals an intense and wide emission band centered at 505 nm. Polarization–electric field (*P–E*) response curves of PTO nanotube array were measured, and the hysteresis loops illustrate a room temperature ferroelectric characteristic of as-prepared PTO nanotubes.



*Keywords:* $PbTiO_3$; Nanotubes; Photoluminescence; Ferroelectricity

## 1. Introduction

Quasi one-dimensional (Q1D) oxide nanostructures, such as nanowires, nanotubes and nanobelts, are attracting more and more attention because of their novel properties compared to their bulk counterparts and potential applications in nanoelectronics, nano-optics and nanodevices [1–4]. To date, most Q1D simple oxides, for example, ZnO, $SiO_2$, $In_2O_3$, $TiO_2$, $SnO_2$, MgO, etc., have been extensively studied [5–16]. Currently, it has an increasing research interest in Q1D multicomponent complex oxides [4,17–25].

In general, the fabrication of Q1D complex oxide nanostructures is relatively difficult through conventional physical or chemical vapor deposition approaches. Although several examples of solution-based syntheses of perovskite nanowires have been reported recently [18,19,25], sol–gel template synthesis, in contrast, has been proven to be a simple and low-cost method for fabricating complex oxide nanowires or nanotubes. Anodic aluminum oxide (AAO) is one of the most widely used templates currently because of its highly ordered nanoporous structure, controllable pore size and excellent chemical stability at high temperature. It is expected that most Q1D complex oxide nanowires or nanotubes can be synthesized via sol–gel template method as long as the ingredient and concentration of precursor sol can be properly controlled and the sol can wet out the nanochannel surfaces of AAO template.

Lead titanate ($PbTiO_3$, PTO) has been widely used in optoelectrics, transducers, sensors and non-volatile memory devices due to its remarkable ferroelectric, pyroelectric and piezoelectric properties [26]. More recently, PTO nanostructures become more and more attractive because they are promising candidates for high-density, non-volatile information storage and scanning

* Corresponding author Present address: Max-Planck Institute of Microstructure Physics, Weinberg 2, D-06120 Halle, Germany. Fax: +49 345 5511 223.

** Corresponding author. Tel.: +86 10 82649081; fax: +86 10 82640215.

*E-mail addresses:* liulif@mpi-halle.mpg.de (L. Liu), ssxie@aphy.iphy.ac.cn (S. Xie).

0921-5107/$ – see front matter © 2007 Elsevier B.V. All rights reserved.
doi:10.1016/j.mseb.2007.12.003

probe-based ferroelectric mass storage [27,28]. Several reports have been dedicated to the synthesis and characterization of PTO nanotubes and nanowires [20,29,30]. In the aspects of physical properties, although size-induced ferroelectric phase transitions of PTO nanotubes has been investigated [22], the photoluminescence (PL) property and polarization–electric field (*P–E*) loops of PTO nanotube arrays are still rarely reported [31]. In this article, we will report the sol–gel template synthesis and structural characterization of PTO nanotubes. Furthermore, photoluminescence and *P–E* loops of PTO nanotube arrays will also be discussed.

## 2. Experimental

The commercially available AAO membranes (Whatman Anodisc 47, nominal pore diameter 200 nm) were used as templates in our experiments. The precursor sol was prepared as follows: 9.552 g lead acetate ($Pb(OAc)_2$, AR) with 5% excess was firstly dissolved in 10 ml glacial acetic acid, and then the solution was refluxed at 60 °C under stirring for 0.5 h. The reason why 5% excess of lead is added in the precursor is to compensate the lead loss during thermal annealing. This has been widely used in the sol–gel synthesis of PTO thin films [22,32,33]. After refluxing, the solution was cooled down to room temperature. A second solution of 7 ml purified $Ti(OPr^i)_4$ and 10 ml ethanol was added to the lead acetate solution drop by drop. Next, the mixed solution was stirred for several hours to obtain clear sol. Then, the AAO template was immersed into the sol. The immersion time was about 3 h. After that, the AAO template was washed carefully with ethanol for several times to remove the residual sol coated on template surfaces, and dried in air for 0.5 h. The AAO template embedded with PTO gel was calcined in air at a rate of 50 °C/h to 650 °C and was maintained at this temperature for 6 h, then was cooled down to room temperature at a rate of 30 °C/h.

The morphology and structure of as-prepared PTO nanotubes were determined by field-emission scanning electron microscope (SEM, Hitachi S-5200), X-ray diffraction (XRD, Riguka) and transmission electron microscope (TEM, JEOL 2010). For SEM and TEM observations, the AAO template embedded with PTO nanotubes was soaked in 4 M NaOH solution for 6 h to remove alumina completely, then the resulting product was washed with distilled water for several times. It was found that the released PTO nanotubes could still keep the closely packed film-like morphology even after removal of the template. Some PTO nanotube films were placed on SEM sample holder to perform morphology observation. For TEM investigation, the film was put in deionized water and subjected to ultrasonic treatment for several minutes, then a drop of suspension was placed on carbon-coated copper grid to carry out TEM studies. The PL spectrum was collected by a fluorescence spectrometer (PTI-C-700) equipped with He–Cd laser ($\lambda = 325$ nm, 50 mW). To measure *P–E* hysteresis loops of PTO nanotube array, both surfaces of the array were firstly polished carefully with sand paper until PTO nanotubes were emerged, and then a layer of Au with a thickness of 100 nm was sputtered on both sides of the template as conductive contacts. The measurement was performed at a nonlinear ferroelectric thin film testing system (Technologies, RT6000S).

## 3. Results and discussion

Fig. 1 shows typical SEM images of as-prepared PTO nanotube array after removal of AAO template. Fig. 1(a) is an overview image of the array. It can be seen that PTO nanotubes still keep aligned morphology even in the absence of the support from AAO template. The length of nanotubes is about 50 μm, consistent with the thickness of template. A close top view SEM image of PTO nanotube array is given in Fig. 1(b). From this picture, the open-ended tubular structure can be clearly seen. The magnified top view image is shown in the inset of Fig. 1(b), illustrating that the average outer diameter and wall thickness of as-prepared nanotubes are about 300 nm and 40 nm, respectively. The particles at the tube mouths are a result of incomplete removal of PTO sol from template surface. Fig. 1(c) displays a side view image of PTO nanotube array. It is evident that the nanotubes are highly parallel to each other and have a closely packed morphology. Fig. 1(d) represents a SEM image taken from the middle part of the nanotube array. The fractures resulted from sample preparation process clearly demonstrate that the nanotubes are hollow through the whole length, instead of just at the ends. Fig. 1(e) shows a representative energy-disperse X-ray (EDX) spectrum of as-prepared PTO nanotubes. It is clear that the nanotubes consist of Pb, Ti and O. The atomic ratio of these three elements is given in the inset of Fig. 1(e), showing that Pb:Ti:O is approximate to 1:1:3. This demonstrates that the as-prepared PTO nanotubes have an ideal stoichiometric ratio.

It is believed that AAO templates we used here played an important role on the formation of nanotubes. As is known, AAO templates have hydrophilic inner surfaces, so the sol entered the nanochannels through capillary action can be easily adsorbed on the channel surfaces, facilitating the tube formation. On the other hand, the 50 μm channel length is too long to allow for more sol solution to enter. Thus, the sol can only fill the nanochannels incompletely, so that solid fibers are difficult to be obtained. In fact, Hernandez et al. have also demonstrated previously that shorter channel length is more conducive to the formation of solid fibers, while using 50-μm thick AAO template yields only nanotubes [22].

The XRD patterns of as-prepared PTO nanotube array embedded in AAO template and PTO gel powders calcined at the same condition are presented in Fig. 2. Since alumina template begins to be crystallized only when it is annealed above 800 °C [34,35], it does not contribute any diffraction peaks in the XRD pattern in present case. From Fig. 2, it is found that all diffraction peaks of PTO gel powders are well consistent with standard powder XRD pattern of tetragonal perovskite PTO (JCPDS 78-0299), and no other impurity phases were detected, which demonstrates the formation of pure tetragonal ferroelectric phase. In contrast, PTO nanotube sample exhibits a similar XRD pattern, but the diffraction peaks of nanotubes are obviously broader. The average crystallite sizes of PTO gel powders and PTO nanotubes are estimated by Scherrer formula after performing proper instrumental broadening correction with $LaB_6$

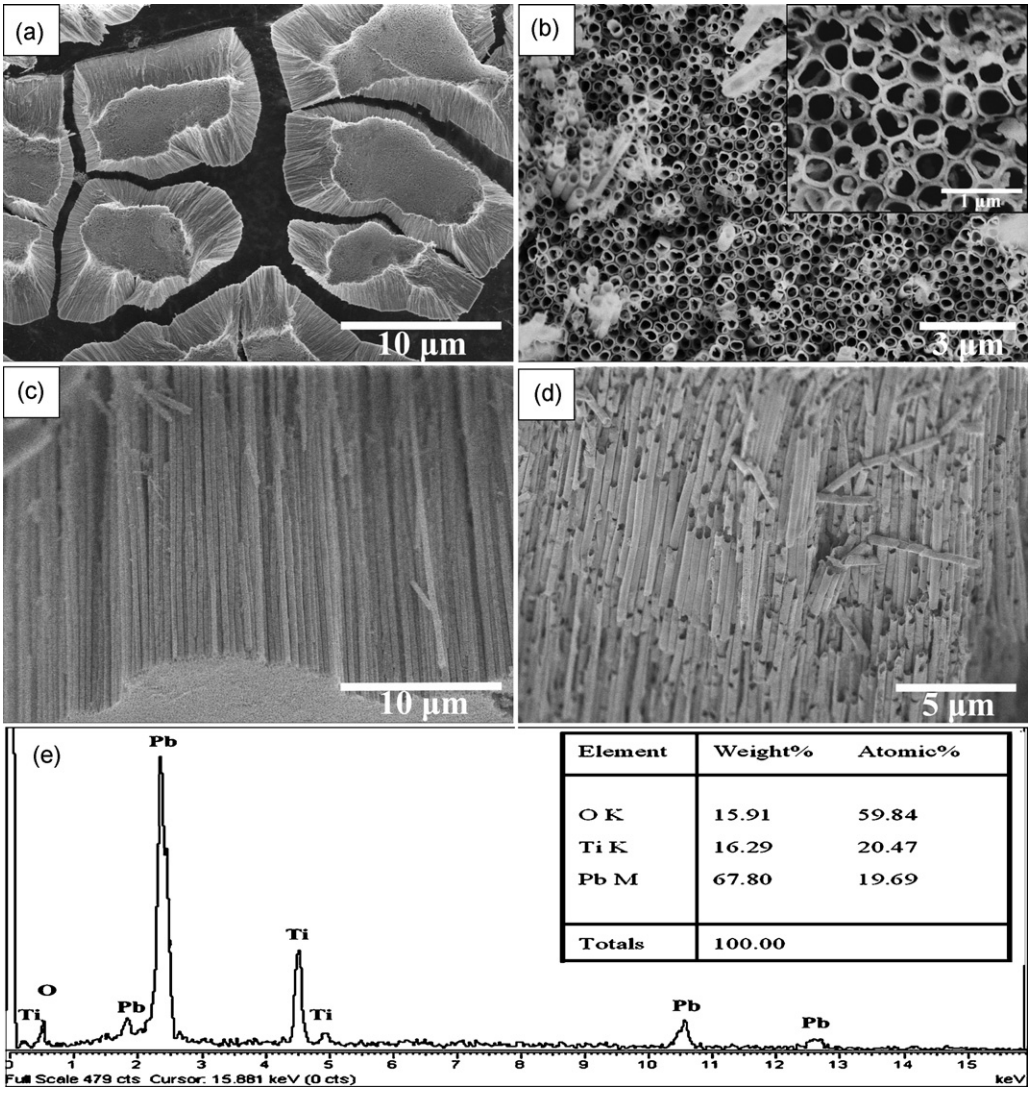


Fig. 1. SEM images of as-prepared PTO nanotubes after the removal of AAO template. (a) Overview; (b) top view, inset: magnified image; (c) side view of the array; (d) SEM image taken from the middle part of the array; (e) EDX spectrum as-prepared PTO nanotubes, inset: the atomic ratio of products.

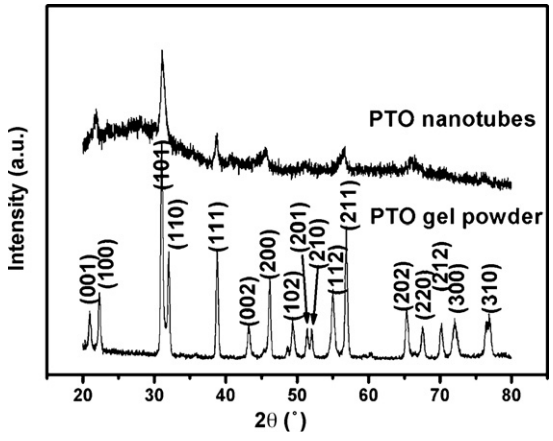


Fig. 2. XRD patterns of as-prepared PTO nanotubes embedded in AAO template and PTO gel powders prepared in the same condition.

standard sample. Scherrer formula can be written as

$$D = \frac{K\lambda}{\beta \cos\theta} \tag{1}$$

where $D$ stands for crystallite size, $K \approx 0.89$ is Scherrer constant, and $\lambda$ and $\beta$ represent the wavelength of X-ray and full width at half maximum of the corresponding diffraction peaks, respectively. Since the shape of PTO nano-crystallites may not be spherical, the crystallite sizes of top three strong diffractions (that is, (1 0 0), (1 1 0) and (1 1 1) diffractions) are calculated and their average value is given. As-calculated average crystallite sizes for PTO gel powders and PTO nanotubes are 69.4 nm and 24.3 nm, respectively. It is evident that the average crystallite size of PTO gel powders is nearly three times larger than that of PTO nanotubes, although they were prepared in the same condition. This implies that AAO template may have a confinement effect on the coalescence of PTO nano-crystallites, as suggested by Hernandez et al. [22]. In addition to small crystallite size, another reason responsible for the XRD peak broadening of PTO

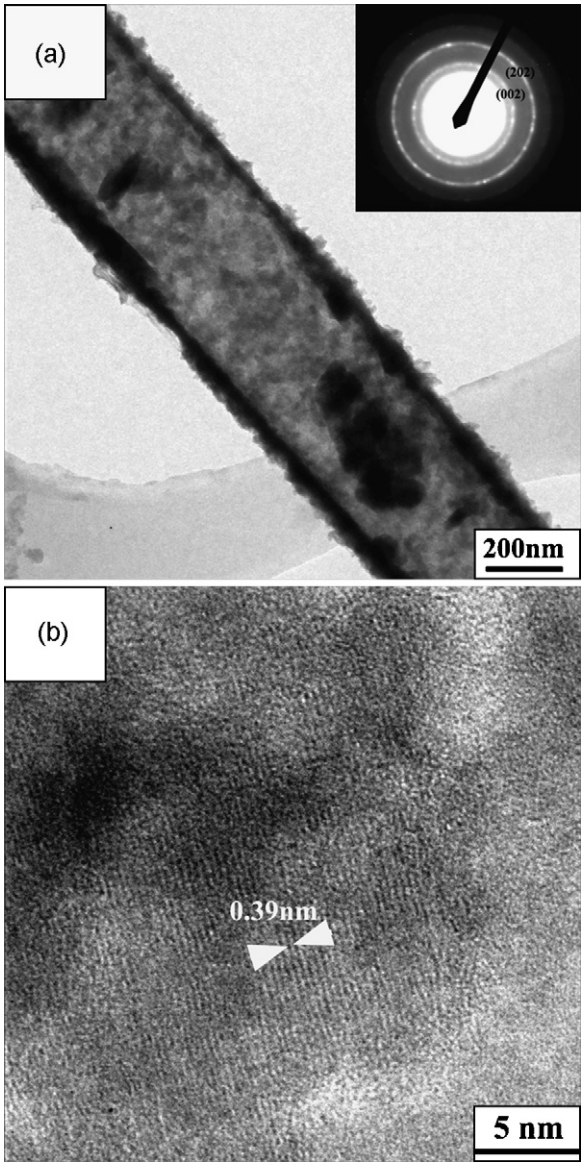


Fig. 3. (a) TEM image of as-prepared PTO nanotubes. Inset: selected-area electron diffraction pattern of PTO nanotubes; (b) HRTEM image of the crystallized region of as-prepared PTO nanotubes.

nanotubes is their poor crystallinity. This will be demonstrated by the HRTEM image shown in Fig. 3(b), which displays the presence of amorphous PTO besides PTO nano-crystallites.

According to Fig. 2, it is also noted that the proximate double-peak diffractions in nanotube sample is disappeared. This seems to imply the formation of cubic paraelectric phase (JCPDS 70-0747) in as-prepared PTO nanotubes. However, it is known that when evaluating nanomaterials via powder XRD method, the effect of line broadening will sometimes cause a pseudocubic structure to be observed [22,36]. Therefore, it could not be concluded readily now that the PTO nanotubes are paraelectric although they reveal a cubic structure. In fact, we noted that similar result was also reported by Hernandez et al. [22]. They clarified that the cubic paraelectric structure of PTO nanotubes determined by XRD was actually a pseudocubic phase caused by line broadening, and they further confirmed the ferroelectric feature of PTO nanotubes by Raman scattering. In our case, we will also demonstrate below that PTO nanotubes we prepared are ferroelectric at room temperature through *P–E* loop measurements.

Fig. 3(a) displays a typical TEM image of as-prepared PTO nanotube. From this picture, it can be seen that the outer diameter of PTO nanotube is uniform along the axial direction, but the wall thickness is inhomogeneous, probably due to the inhomogeneous covering of precursor sol on the channel surfaces. The electron diffraction pattern is given in the inset of Fig. 3(a). The ring-like diffractions clearly demonstrate the polycrystalline character of as-prepared nanotubes, which is in agreement with XRD data. For obtaining further insight about the microstructures of the nanotubes, HRTEM was performed. It is found that the nanotubes actually consist of many PTO nano-crystallites dispersed in amorphous PTO matrix. One of representative HRTEM images of the crystallites is shown in Fig. 3(b). The interplanar distance of the crystallite is about 0.39 nm, corresponding to that of PTO (1 0 0) crystal planes. The average size of the crystallites is approximate to 20 nm, slightly smaller than that calculated by Scherrer formula (24.3 nm).

Although perovskite-type titanates have been extensively studied for many years, their PL properties were neglected. Until recently, the discovery of room temperature PL emission in amorphous $ABO_3$ perovskites stimulates considerable research interests in room temperature PL of this class of materials [37–43]. Here, room temperature PL behavior of as-prepared PTO nanotubes embedded in AAO template is investigated. For reference, the PL spectra of empty AAO template as well as PTO gel powders are also given. Fig. 4(a) and (b) shows the PL spectra of AAO template and PTO nanotubes embedded in template, respectively. As is depicted in Fig. 4(a), two broad emission bands centered at 408 nm and 455 nm were detected. In contrast, the PL spectrum of PTO nanotubes embedded in template can be fitted with three bands centered at 407 nm, 455 nm and 505 nm, respectively, just like the dash curves shown in Fig. 4(b). Compared with Fig. 4(a), it is evident that the first two PL bands are originated from the emission of AAO template, while the last band centered at 505 nm is the emission of PTO nanotubes themselves. Fig. 4(c) displays the PL spectrum of well-crystallized PTO gel powders (as shown in Fig. 2). No PL peaks can be detected except the background of excited light source. This agrees well with previous reports [37–43], which have demonstrated that room temperature PL cannot be observed in well-crystallized $ABO_3$ materials.

Now there is a consensus that room temperature PL emission of amorphous $ABO_3$ materials is mainly originated from their structural disorder [43]. We consider that this should also be the origin of room temperature PL of PTO nanotubes studied here. As we can see from Fig. 3(b), the PTO nanotubes consist of small PTO nano-crystallites dispersed in amorphous PTO matrix. Such structural disorder will result in a non-uniform band gap structure [37–40]. On one hand, the presence of amorphous PTO will introduce localized tail states in which electrons or holes may be trapped. On the other hand, it has been demonstrated both experimentally and theoretically that there exist two kinds of Ti coordination in amorphous PTO, fivefold oxy-

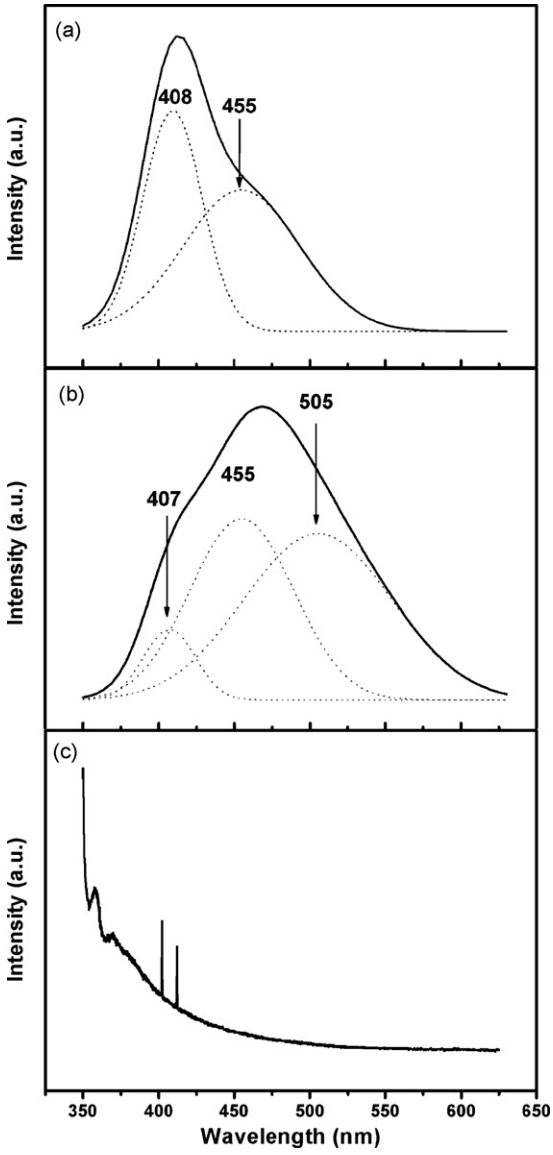


Fig. 4. Photoluminescence spectra of (a) AAO template; (b) PTO nanotubes embedded in AAO template; (c) well-crystallized PTO gel powders.

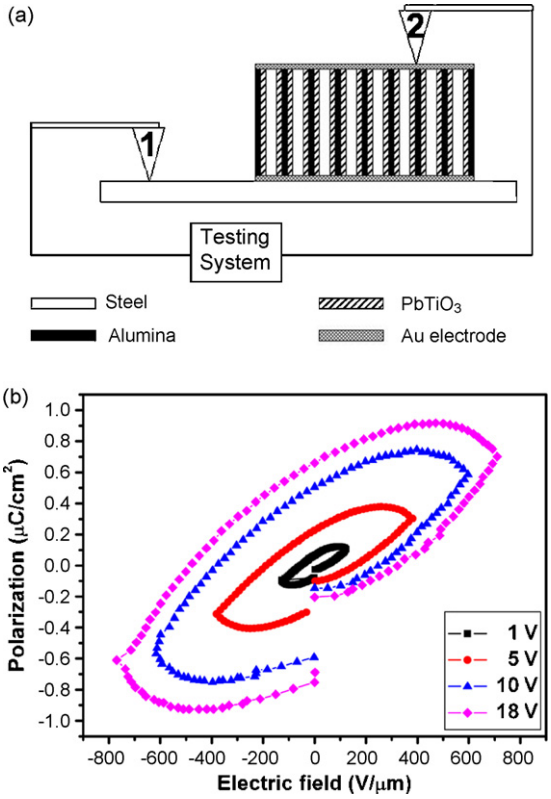


Fig. 5. (a) The schematic diagram of *P–E* loop measurement of PTO nanotube array; (b) *P–E* hysteresis loops of PTO nanotube array measured with different voltage ranges.

gen Ti coordination ($TiO_5$ square base pyramid) and sixfold oxygen Ti coordination ($TiO_6$ octahedron) [40,42]. The coexistence of [$TiO_5$] and [$TiO_6$] clusters will yield a charge imbalance that encourages the trapping of holes in previously mentioned localized states. In addition, a large amount of surface defects and oxygen vacancies are usually existed in sol–gel synthesized materials, and consequently yield gap states. Since the PL emission of PTO nanotubes is centered at 505 nm (2.46 eV), It could not result from the direct energy gap transition because the band gaps of PTO ceramic and sol–gel-derived films are around 3.6 eV [44]. Thus, the photoluminescence of PTO nanotubes may be attributed to the radiative recombination between trapped electrons and trapped holes in tail and gap states. This radiative recombination mechanism of PL emission in amorphous PTO nanomaterials has been proven by Leite et al. [39,42,43].

For investigating the ferroelectric feature of as-prepared PTO nanotubes, the *P–E* loops of nanotube array were measured at room temperature. Fig. 5(a) is the schematic diagram of *P–E* curve measurement. The sample stage and two probes are made of stainless steel. One of probes (probe 1) always kept contact with sample stage during the measurement, so that they had equal potential. The PTO nanotube array embedded in AAO template with top and bottom Au electrodes was directly placed on the surface of sample stage, thus, the bottom electrode also got a same potential with sample stage and probe 1. Then another probe (probe 2) was drived to approach the top electrode of PTO nanotube array. A capacitance detector was applied between the two probes to monitor the capacitance between probe 2 and top electrode. When probe 2 did not touch the top electrode, the detector shown the capacitance of the air. But when probe 2 had a good contact with top electrode, the capacitance would have a sharp change. At this point, the measurement could start. *P–E* loops measured within different voltage ranges are displayed in Fig. 5(b). Here, the polarization values have been normalized to the area fraction of PTO nanotubes. The hysteresis behavior unambiguously demonstrates the room temperature ferroelectricity of as-prepared PTO nanotubes. It also clarifies that the cubic structure of PTO nanotubes determined by XRD does represent "pseudocubic" phase, and is not a real paraelectric phase. From Fig. 5(b), it also can be seen that the hysteresis can even occur when the applied voltage changes only within a small range of −1 V to +1 V, indicating that the PTO nanotubes are easily polarized. With the increase of applied voltage range, both remanent polarization and coercive field enlarge gradually.

However, leaky behavior is shown when high voltage is applied, as can be seen from the bending corner of *P–E* loops at extreme applied voltage.

We also prepared PTO nanotubes with different diameter and wall thickness successfully. This was achieved by varying pore diameter of template and the immersion time of AAO template in precursor sol. The investigation about the influence of diameter and wall thickness on photoluminescence and ferroelectric properties is in progress.

## 4. Conclusion

In summary, we have successfully prepared PTO nanotube array via sol–gel template approach. The morphology and structures were investigated by SEM, XRD and TEM in detail. Room temperature PL property of as-prepared PTO nanotubes was studied, and a wide PL band centered at 505 nm was detected. It is considered that the luminescence emission is attributed to the polycrystalline microstructures and is originated from the radiative recombination of trapped electrons and holes in tail and gap states. Furthermore, *P–E* loops of as-prepared PTO nanotube array were measured, and the hysteresis clearly demonstrates the room temperature ferroelectricity of the nanotubes, indicating PTO nanotube array is potential media as ferroelectric information storage.

## Acknowledgements

The authors thank Mr. J.R. Chen for his help in XRD measurement, Mr. X.A. Yang for his assistance in TEM experiment and Mr. Q.S. Zeng for his help in PL measurement. L.F. Liu also thanks Z.X. Zhang and Y.J. Xiang for their helps in the experiment. This work was supported by National Natural Science Foundation of China (Grant No. 10334060) and "973" National Key Basic Research Program of China (Grant No. 2005CB623603).

## References

[1] M. Remskar, Adv. Mater. 16 (2004) 1497.
[2] C.N.R. Rao, F.L. Deepak, G. Gundiah, A. Govindaraj, Prog. Solid State Chem. 31 (2003) 5.
[3] Z.L. Wang, Adv. Mater. 15 (2003) 1487.
[4] K. Shantha, A.K. Shankar, Raychaudhuri, Mater. Sci. Eng. C 25 (2005) 738.
[5] Z.L. Wang, J. Phys. Condens. Mater. 16 (2004) R829.
[6] M.H. Huang, S. Mao, H. Feick, H.Q. Yan, Y.Y. Wu, H. Kind, W. Weber, R. Russo, P.D. Yang, Science 292 (2002) 1897.
[7] S. Kar, A. Dev, S. Chaudhuri, J. Phys. Chem. B 110 (2006) 17848.
[8] S. Kar, B.N. Pal, S. Chaudhuri, D. Chakravorty, J. Phys. Chem. B 110 (2006) 4605.
[9] D.P. Yu, Q.L. Hang, Y. Ding, H.Z. Zhang, Z.G. Bai, J.J. Wang, Y.H. Zou, W. Qian, G.C. Xiong, S.Q. Feng, Appl. Phys. Lett. 73 (1998) 3076.
[10] P. Guha, S. Kar, S. Chaudhuri, Appl. Phys. Lett. 85 (2004) 3851.
[11] S. Kar, S. Chakrabarti, S. Chaudhuri, Nanotechnology 17 (2006) 3058.
[12] C. Li, D.H. Zhang, X.L. Liu, S. Han, T. Tang, J. Han, C.W. Zhou, Appl. Phys. Lett. 82 (2003) 1613.
[13] Y. Lei, L.D. Zhang, G.W. Meng, G.H. Li, X.Y. Zhang, C.H. Liang, W. Chen, S.X. Wang, Appl. Phys. Lett. 78 (2001) 1125.
[14] Z.R. Dai, J.L. Gole, J.D. Stout, Z.L. Wang, J. Phys. Chem. B 106 (2002) 1274.
[15] S. Kar, S. Chaudhuri, J. Nanosci. Nanotechnol. 6 (2006) 1447.
[16] Y.D. Yin, G.T. Zhang, Y.N. Xia, Adv. Funct. Mater. 12 (2002) 293.
[17] Y.F. Zhang, Y.H. Tang, X.F. Duan, Y. Zhang, C.S. Lee, N. Wang, I. Bello, S.T. Lee, Chem. Phys. Lett. 323 (2000) 180.
[18] J.J. Urban, W.S. Yun, Q. Gu, H. Park, J. Am. Chem. Soc. 124 (2002) 1186.
[19] J.J. Urban, J.E. Spanier, L. Ouyang, W.S. Yun, H. Park, Adv. Mater. 15 (2003) 423.
[20] B.A. Hernandez, K.S. Chang, E.R. Fisher, P.K. Dorhout, Chem. Mater. 14 (2002) 480.
[21] J. Curiale, R.D. Sanchez, H.E. Troiani, H. Pastoriza, P. Levy, A.G. Leyva, Physica B 354 (2004) 98.
[22] B.A. Hernandez-Sanchez, K.S. Chang, M.T. Scancella, J.L. Burris, S. Kohli, E.R. Fisher, P.K. Dorhout, Chem. Mater. 17 (2005) 5909.
[23] Z.A. Hu, H.Y. Wu, X.L. Shang, R.J. Lu, H.L. Li, Mater. Res. Bull. 41 (2006) 1045.
[24] Z. Yang, Y. Huang, B. Dong, H.L. Li, S.Q. Shi, Appl. Phys. A 84 (2006) 117.
[25] H. Liu, C.G. Hu, Z.L. Wang, Nano Lett. 6 (2006) 1535.
[26] M. Okuyama, Y. Hamakawa, Int. J. Eng. Sci. 29 (1991) 391.
[27] S. Clemens, T. Schneller, A. van der Hart, F. Peter, R. Waser, Adv. Mater. 17 (2005) 1357.
[28] S. Clemens, T. Schneller, R. Waser, A. Rudiger, F. Peter, S. Kronholz, T. Schmitz, S. Tiedke, Appl. Phys. Lett. 87 (2005) 142904.
[29] Y. Deng, J.L. Wang, K.R. Zhu, M.S. Zhang, J.M. Hong, Q.R. Gu, Z. Yin, Mater. Lett. 59 (2005) 3272.
[30] M.C. Hsu, I.C. Leu, Y.M. Sun, M.H. Hon, J. Solid State Chem. 179 (2006) 1421.
[31] Y.M. Hu, H.S. Gu, X.C. Sun, J. You, J. Wang, Appl. Phys. Lett. 88 (2006) 193120.
[32] V.E. Wood, J.R. Busch, S.D. Ramamurthi, S.L. Swartz, J. Appl. Phys. 71 (1992) 4557.
[33] S.D. Cheng, C.H. Kam, Y. Zhou, W.X. Que, Y.L. Lam, Y.C. Chan, W.S. Gan, Thin Solid Films 375 (2000) 109.
[34] T. Li, S. Yang, L. Huang, J. Zhang, B. Gu, Y. Du, J. Phys. Condens. Mater. 16 (2004) 2463.
[35] X. Sun, F. Xu, Z. Li, W. Zhang, J. Lumin. 121 (2006) 588.
[36] B.D. Cullity, Elements of X-ray Diffraction, Addision-Wesley, Reading, MA, 1978.
[37] P.S. Pizani, E.R. Leite, F.M. Pontes, E.C. Paris, J.H. Rangel, E.J.H. Lee, E. Longo, P. Delega, J.A. Varela, Appl. Phys. Lett. 77 (2000) 824.
[38] E.R. Leite, L.P.S. Santos, N.L.V. Carreno, E. Longo, C.A. Paskocimas, J.A. Varela, F. Lanciotti, C.E.M. Campos, P.S. Pizani, Appl. Phys. Lett. 78 (2001) 2148.
[39] E.R. Leite, F.M. Pontes, E.C. Paris, C.A. Paskocimas, E.J.H. Lee, E. Longo, P.S. Pizani, J.A. Varela, V. Mastelaro, Adv. Mater. Opt. Electron. 10 (2003) 235.
[40] E.R. Leite, E.C. Paris, F.M. Pontes, C.A. Paskocimas, E. Longo, F. Sensato, C.D. Pinheiro, J.A. Varela, P.S. Pizani, C.E.M. Campos, F. Lanciotti Jr., J. Mater. Sci. 38 (2003) 1175.
[41] P.S. Pizani, E.R. Leite, F.M. Pontes, E.C. Paris, J.H. Rangel, E.J.H. Lee, E. Longo, P. Delega, J.A. Varela, Appl. Phys. Lett. 77 (2006) 824.
[42] M. Anicete-Santos, M.S. Silva, E. Orhan, M.S. Goes, M.A. Zaghete, C.O. Paiva-Santos, P.S. Pizani, M. Cilense, J.A. Varela, E. Longo, J. Lumin. 127 (2007) 689.
[43] E. Orhan, F.M. Pontes, M.A. Santos, E.R. Leite, A. Beltran, J. Andres, T.M. Boschi, P.S. Pizani, J.A. Varela, C.A. Taft, E. Longo, J. Phys. Chem. B 108 (2004) 9221.
[44] D.H. Bao, X. Yao, K. Shinozaki, N. Mizutani, J. Phys. D: Appl. Phys. 36 (2003) 2141.